Supporting Information

Efficient emission quasi-two-dimensional perovskite films casted by ink-jet printing for pixel-defined matrix light-emitting diodes

Junjie Wang[1], Danyang Li[1], Jian Wang[1], Junbiao Peng[1,*]

[1]Institute of Polymer Optoelectronic Materials and Devices, State Key Laboratory of Luminescent Materials and Devices, South China University of Technology, Guangzhou 510640, China.

* E-Mail: psjbpeng@scut.edu.cn

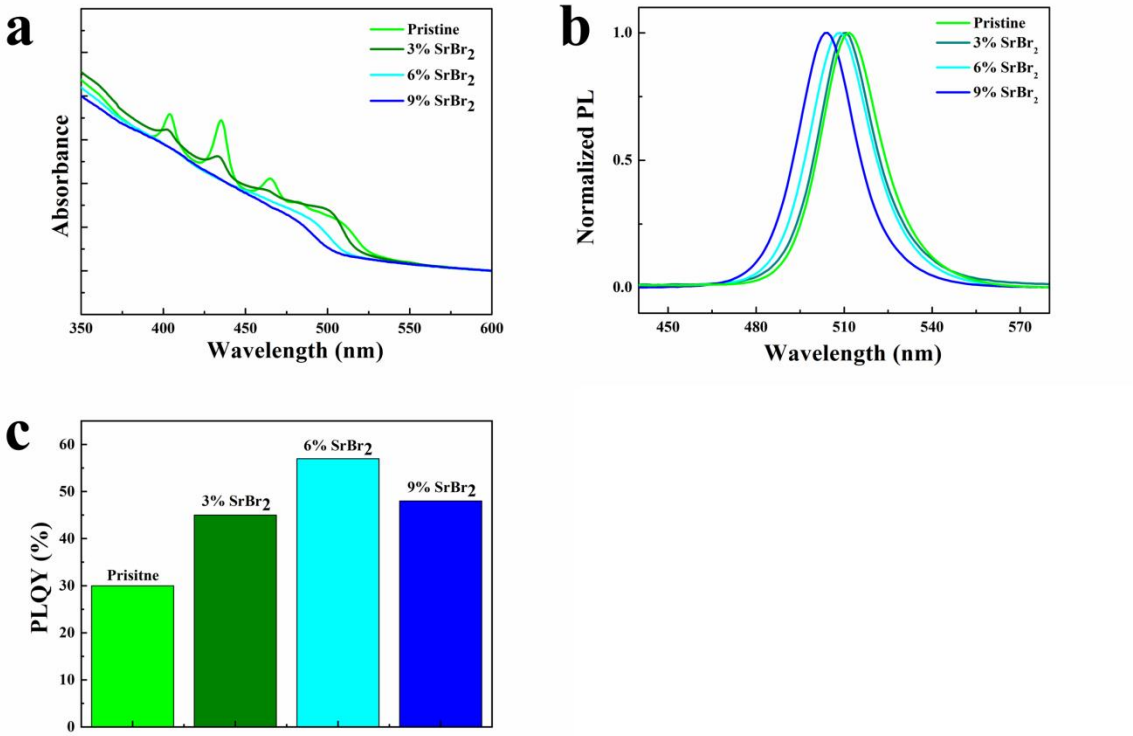

Figure S1. (a) Absorption spectra, (b) PL spectra and (c) PLQY of perovskite films with different $SrBr_2$ proportions.

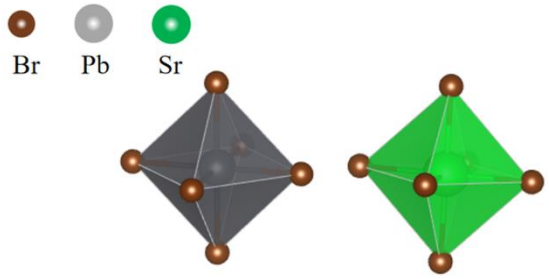

Pb^{2+}	Sr^{2+}	Br^-	$[PbBr_6]^{4-}$	$[SrBr_6]^{4-}$	Octahedral formation energy of ($[PbBr_6]^{4-}$)	Octahedral formation energy of ($[SrBr_6]^{4-}$)
14.486 eV	11.422 eV	-4.976 eV	-29.178 eV	-30.956 eV	-13.808 eV	-12.522 eV

Octahedral formation energy of ($[ABr_6]^{4-}$) = $[ABr_6]^{4-}$ -A^{2+}-6 Br^-

Figure S2. Octahedral formation energy calculation results of $[PbBr_6]^{4-}$ and $[SrBr_6]^{4-}$ by DFT.

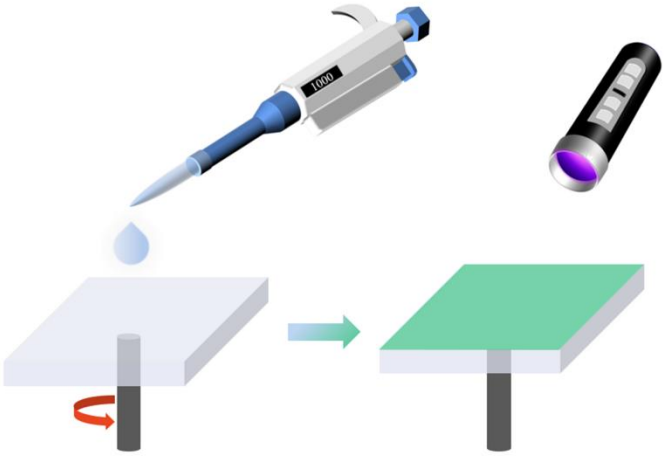

	Time (s)	condition
pristine	27	0.2 M 26.5 ℃ 4000 rpm
6% $PbBr_2$	26	
6% $MgBr_2$	45	
6% $CaBr_2$	41	
6% $SrBr_2$	36	
6% $BaBr_2$	34	

Figure S3. Schematic illustration of the spin-coating process for perovskite films on quartz substrate and crystallizing time.

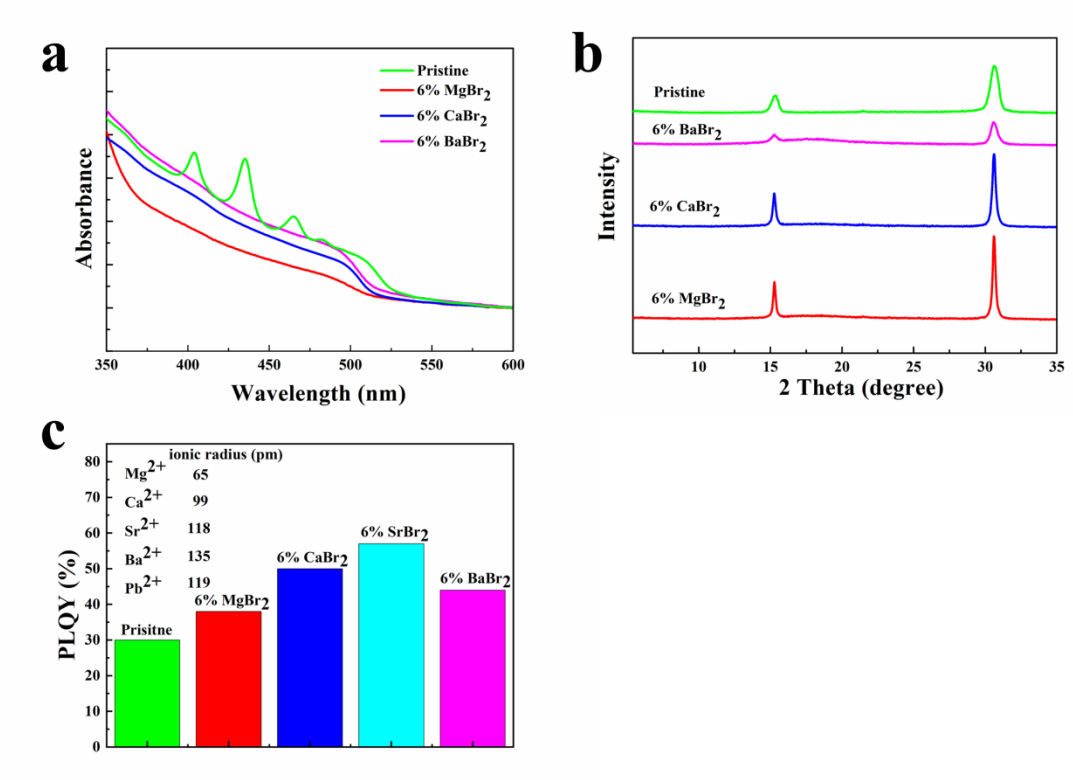

Figure S4. (a) Absorption spectra of quasi-2D perovskite films with 6% $MgBr_2$, 6% $CaBr_2$, 6% $BaBr_2$, (b) XRD spectra of quasi-2D perovskite films with 6% $MgBr_2$, 6% $CaBr_2$, 6% $BaBr_2$, (c) PLYQ of quasi-2D perovskite films with 6% $MgBr_2$, 6% $CaBr_2$, 6% $SrBr_2$, 6% $BaBr_2$.

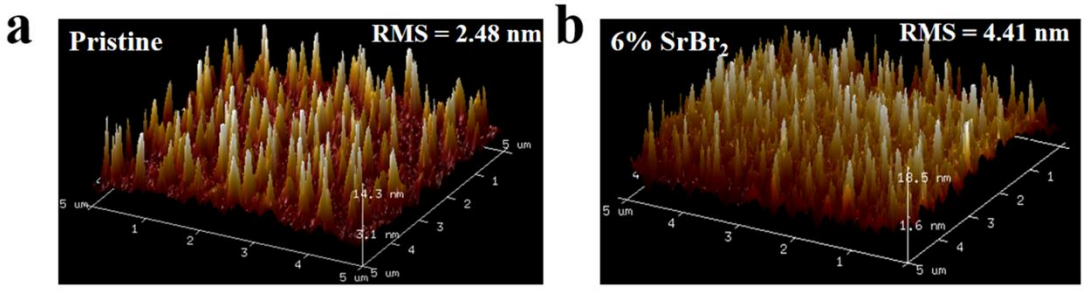

Figure S5. Atomic force microscope images of perovskite film, (a) without and (b) with 6% $SrBr_2$.

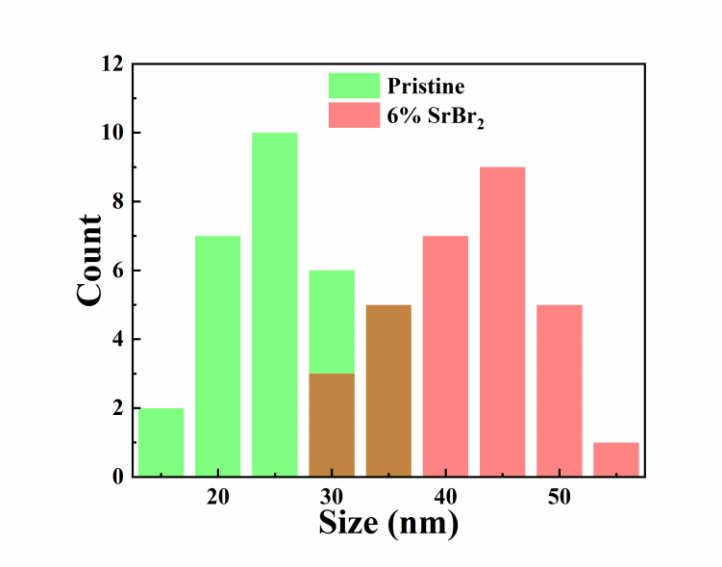

Figure S6. The histogram of grain size distribution.

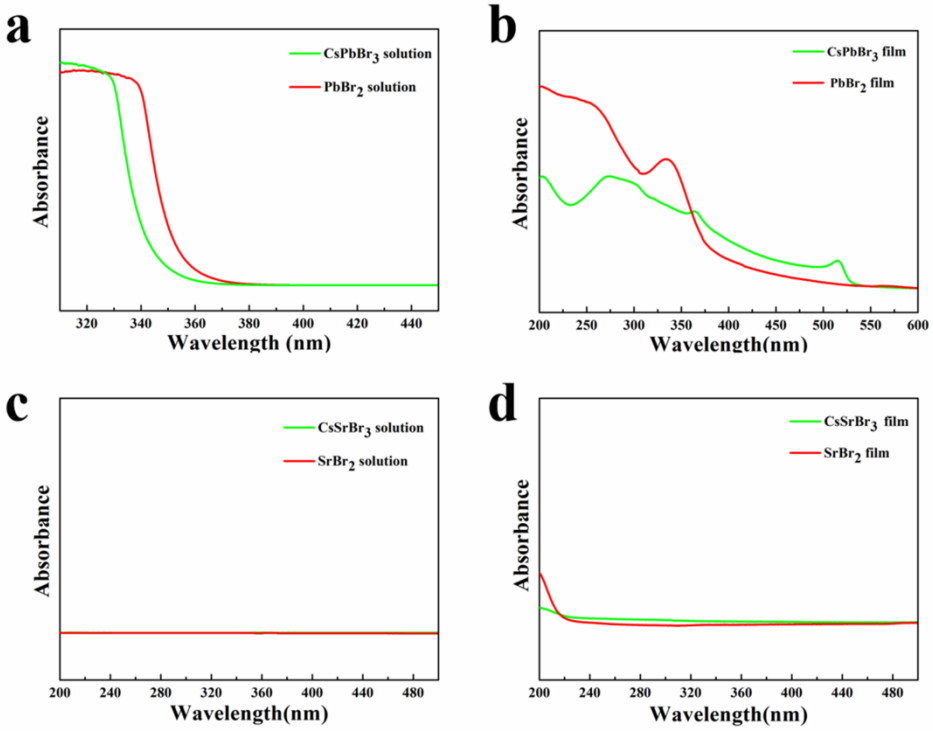

Figure S7. Absorption spectra of (a) $CsPbBr_3$ and $PbBr_2$ in DMSO, (b) $CsPbBr_3$ film and $PbBr_2$ film, (c) $CsSrBr_3$ and $SrBr_2$ in DMSO, (d) $CsSrBr_3$ film and $SrBr_2$ film.

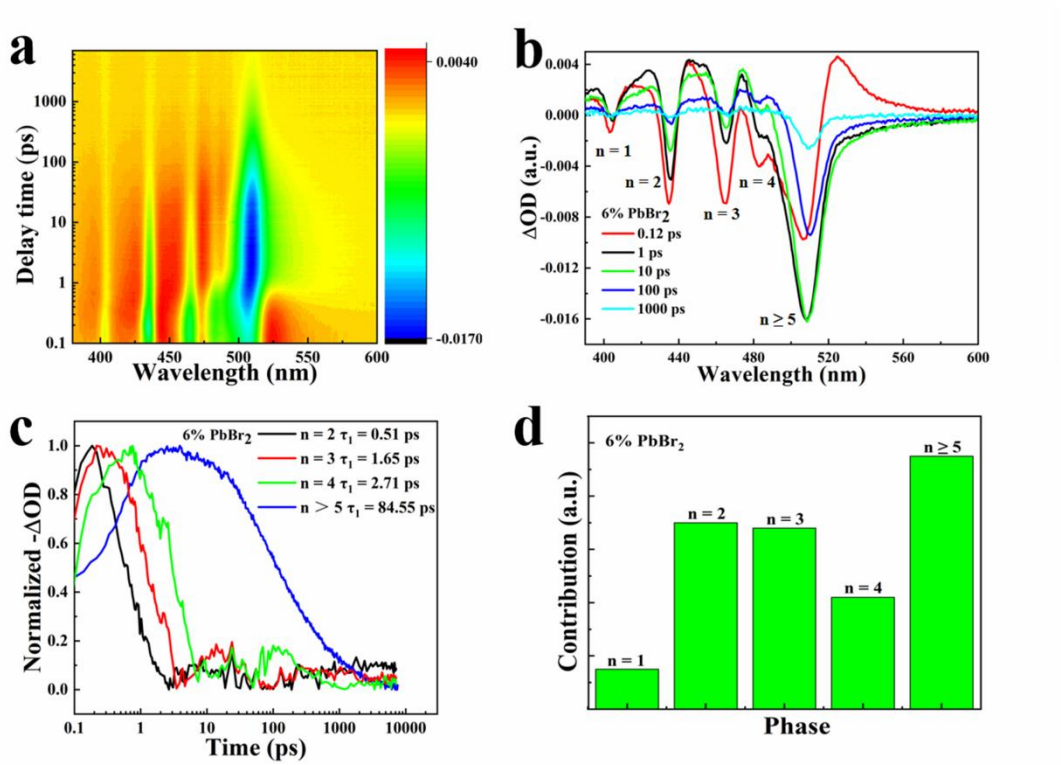

Figure S8. (a) TA spectra, (b) TA spectra at selected timescales, (c) TA traces as a function of time and extracted fast component decay constants (τ_1) for different phases, (d) Relative contents of different phases for quasi-2D perovskite films with 6% $PbBr_2$, the relative contents were obtained according to the amplitude of GSBs in TA spectra at 0.12 ps.

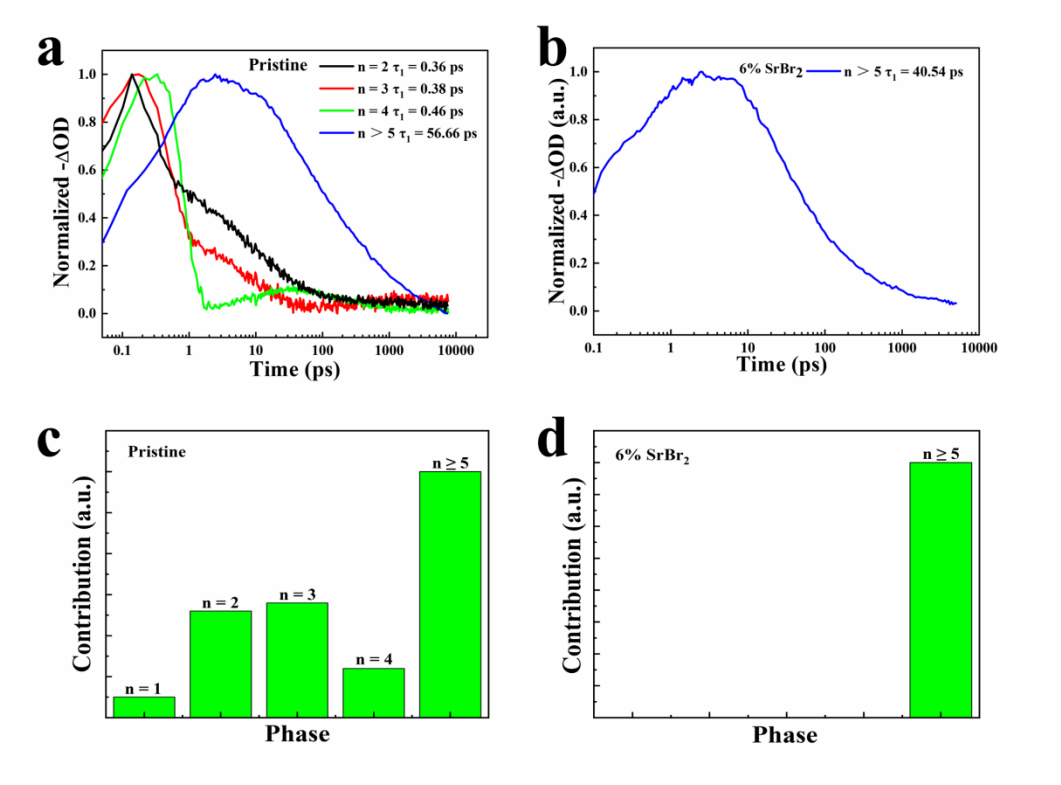

Figure S9. TA traces as a function of time and extracted fast component decay constants (τ_1) for different phases (a) without and (b) with 6% $SrBr_2$. Relative contents of different phases for quasi-2D perovskite films (c) without and (d) with 6% $SrBr_2$, the relative contents obtained according to the amplitude of GSBs in TA spectra at 0.12 ps.

	τ_{au} (ns)	τ_1 (ns)	A_1	τ_2 (ns)	A_2	τ_3 (ns)	A_3
Pristine	26.2	8.0	39%	52.0	44%	1.4	17%
6% $PbBr_2$	16.0	1.3	23%	6.4	43%	38.2	34%
6% $SrBr_2$	39.5	13.3	39%	68.0	50%	2.6	11%

Figure S10. TRPL fitting data of perovskite films without additive, with 6% $PbBr_2$ and with 6% $SrBr_2$, respectively.

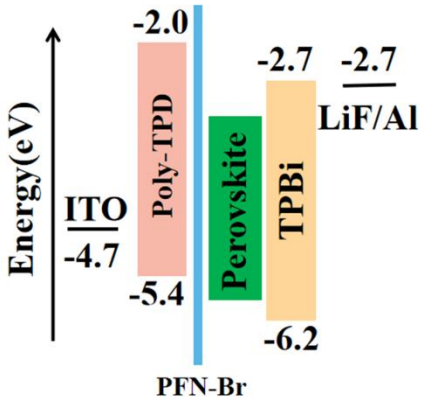

Figure S11. Energy level diagram of the PeLED device structure.

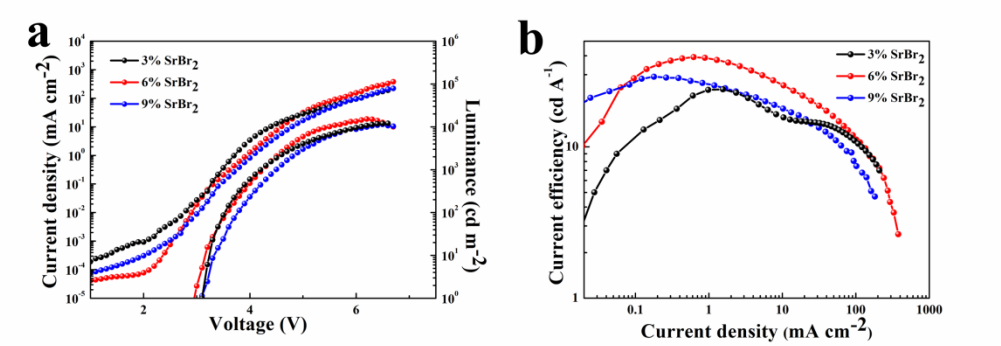

	V_{on} (V)	L_{max} (cd m^{-2})	EL peak (nm)	CE_{max} (cd A^{-1})	EQE(%)
3% $SrBr_2$	3.0	12064	510	24.0	8.2
6% $SrBr_2$	2.9	15194	509	39.2	13.9
9% $SrBr_2$	3.0	11406	507	29.1	11.0

Figure S12. (a) Current density–voltage–luminance, (b) current efficiency–current density curves, and (c) EL spectra of PeLEDs with different $SrBr_2$ proportions.

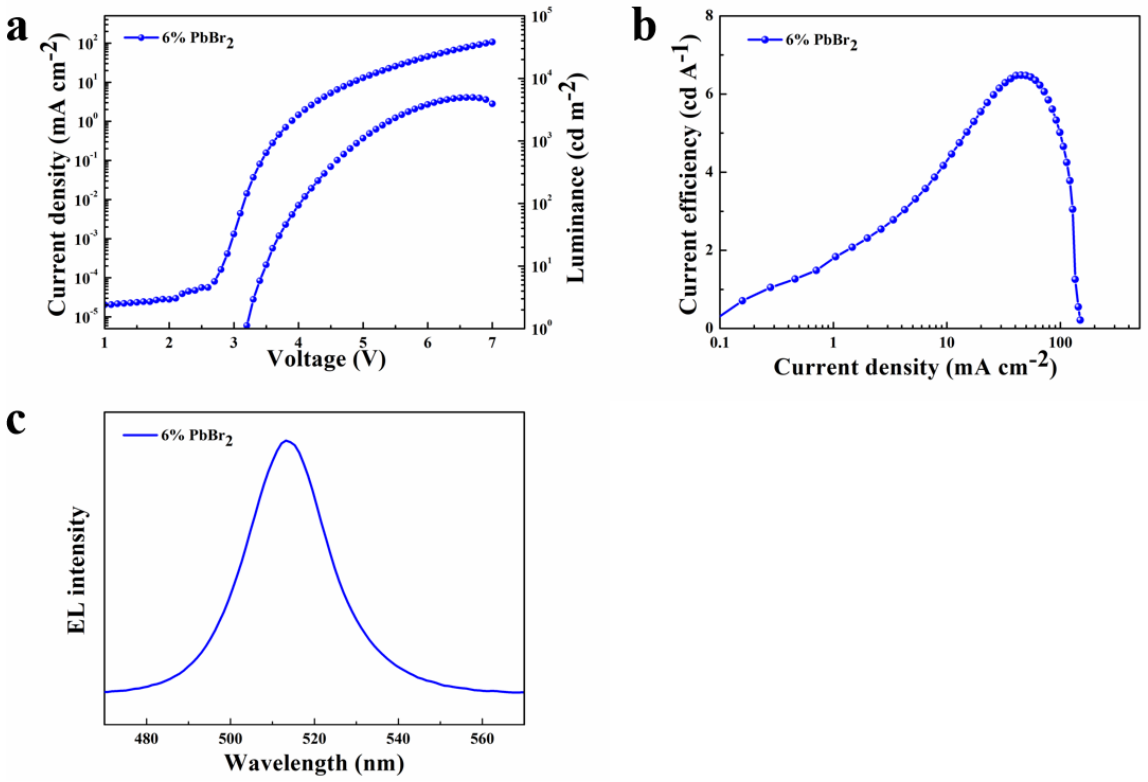

Figure S13. (a) Current density–voltage–luminance, (b) current efficiency–current density curves, and (c) EL spectra of PeLEDs with 6% $PbBr_2$.

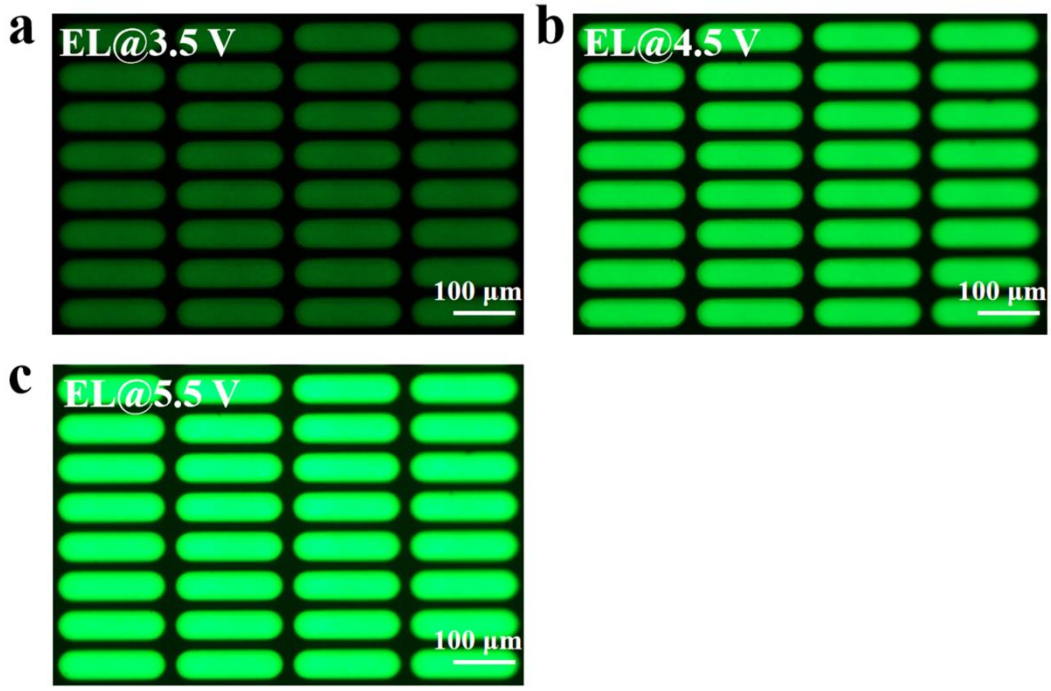

.

Figure S14. (a-c) EL images of perovskite film pixel under a driven voltage of 3.5V, 4.5V, and 5.5 V, respectively.

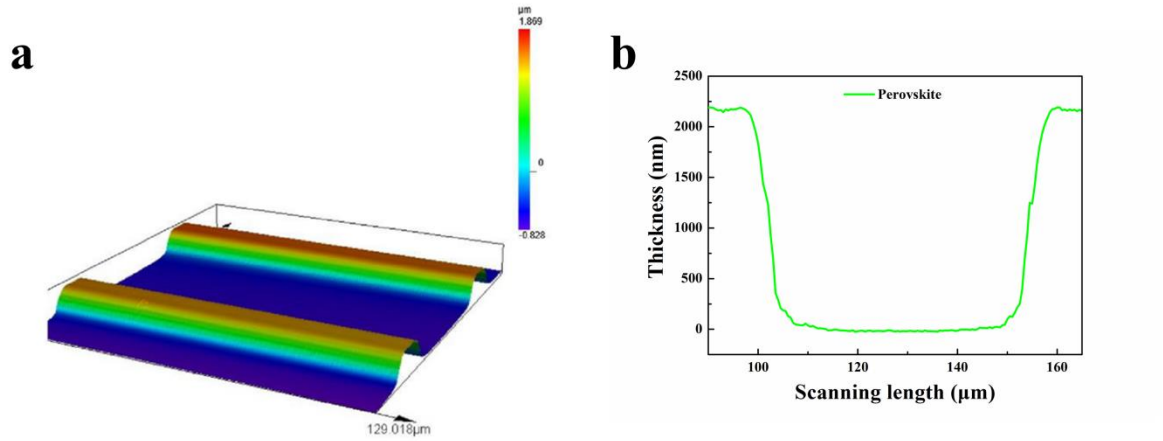

Figure S15. (a, b) The confocal images of perovskite film.

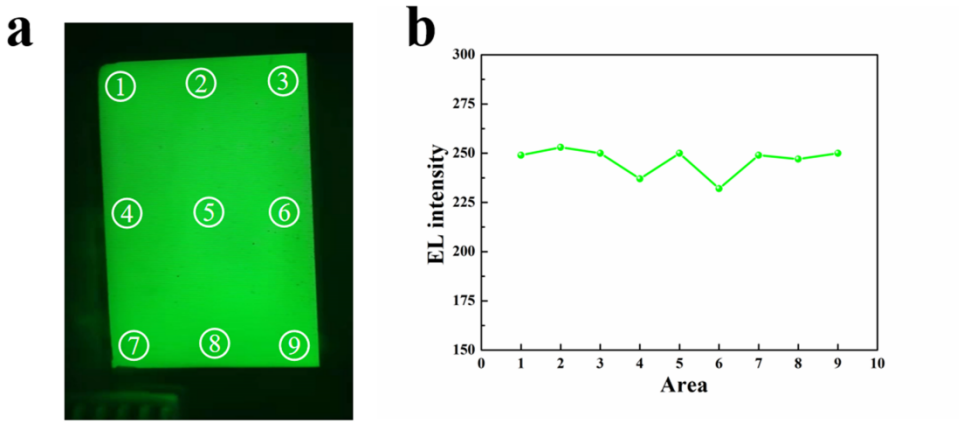

Figure S16. (a) Photo of a working PeLED device operated under voltage of 4.5 V with an active area of 10.0 cm^2, (b) EL intensity curves of the selected micro-areas marked in (a).

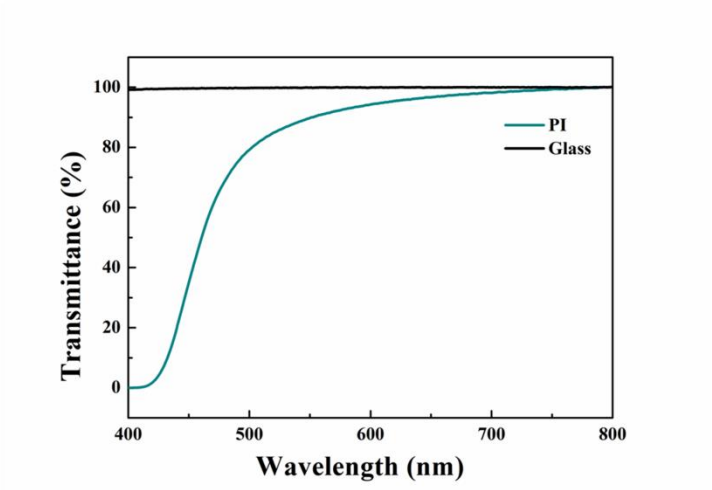

Figure S17. Transmittance of glass and PI substrates.

Table S1. Comparison of device performances for PeLEDs based on ink-jet printing technology reported to date.

Type of Perovskites	Substrate type	Wavelength (nm)	Peak EQE (%)	Area (cm^2)	References
Nanocrystal	Patterned	520	2.8	0.1	1
Nanocrystal	Patterned	515	3.03	0.04	2
3D	W/O Patterned	530	-	0.04	3
Quasi-2D	W/O Patterned	518	9.0	0.09	4
Nanocrystal	W/O Patterned	517	8.54	0.04	5
3D	W/O Patterned	535	2.01 cd A^{-1}	-	6
Quasi-2D	Patterned	645	3.5	0.1	7
		515	3.4		
		486	1.0		
Nanocrystal	Patterned	646	9.6	0.1	8
Quasi-2D	Patterned	511	10.1	0.1	9
Quasi-2D	**Patterned**	**509**	**13.9**	**0.1**	**This work**
			9.3	**10.0**	

References

[1] D. Li, J. Wang, M. Li, G. Xie, B. Guo, L. Mu, H. Li, J. Wang, H.-L. Yip, J. Peng. *Adv. Mater. Technol*. **2020**, *5*, 2000099.

[2] C. Zheng, X. Zheng, C. Feng, S. Ju, Z. Xu, Y. Ye, T. Guo, F. Li. *Organic Electronics*. **2021**, *93*, 106168.

[3] F. Hermerschmidt, F. Mathies, V. R. F. Schröder, C. Rehermann, N. Z. Morales, E. L. Unger, E. J. W. List-Kratochvil. *Mater. Horiz*. **2020**, *7*, 1773.

[4] Y. Li, Z. Chen, D. Liang, J. Zang, Z. Song, L. Cai, Y. Zou, X. Wang, Y. Wang, P. Li, X. Gao, Z. Ma, X. Mu, A. El-Shaer, L. Xie, W. Su, T. Song, B. Sun. *Adv. Optical. Mater*. **2021**, *6*, 2100553.

[5] C. Wei, W. Su, J. Li, B. Xu, Q. Shan, Y. Wu, F. Zhang, M. Luo, H. Xiang, Z. Cui, H. Zeng. *Adv. Mater*, **2022**, 3*4*, 2107798.

[6] J. Zhao, L.-W. Lo, H. Wan, P. Mao, Z. Yu, C. Wang. *Adv. Mater*. **2021**, *33*, 2102095.

[7] J. Wang, D. Li, L. Mu, M. Li, Y. Luo, B. Zhang, C. Mai, B. Guo, L. Lan, J. Wang, H.-L. Yip, J. Peng. *ACS Appl. Mater. Interfaces* **2021**, *13*, 41773.

[8] D. Li, J. Wang, M. Li, B. Guo, L. Mu, Y. Luo, Y. Xiao, C. Mai, J. Wang, J. Peng. *Mater. Futures* **2022**, *1*, 015301.

[9] J. Wang, D. Li, Y. Luo, J. Wang, J. Peng. *Adv. Mater. Technol*. **2022**, 2200370. DOI: 10.1002/admt.202200370.